ACS APPLIED MATERIALS & INTERFACES

Research Article

www.acsami.org

Anomalous Stagewise Lithiation of Gold-Coated Silicon Nanowires: A Combined In Situ Characterization and First-Principles Study

Chia-Yun Chou,[†,‡] Jong-Hyun Seo,[†,§] Yu-Hao Tsai,[‡] Jae-Pyoung Ahn,[§] Eunsu Paek,[⊥] Mann-Ho Cho,[∥] In-Suk Choi,[*,#] and Gyeong S. Hwang[*,‡,⊥]

[‡]Materials Science and Engineering Program and [⊥]McKetta Department of Chemical Engineering, University of Texas at Austin, Austin, Texas 78712, United States

[§]Advanced Analysis Center and [#]High Temperature Energy Materials Research Center, Korea Institute of Science and Technology, Seoul 130-650, South Korea

[∥]Institute of Physics and Applied Physics, Yonsei University, Seoul 120-749, Korea

ABSTRACT: Through a combined density functional theory and in situ scanning electron microscopy study, the effects of presence of gold (Au) spreading on the lithiation process of silicon nanowire (SiNW) were systematically examined. Different from a pristine SiNW, an Au-coated SiNW (Au-SiNW) is lithiated in three distinct stages; Li atoms are found to be incorporated preferentially in the Au shell, whereas the thin AuSi interface layer may serve as a facile diffusion path along the nanowire axial direction, followed by the prompt lithiation of the Si core in the radial direction. The underlying mechanism of the intriguing stagewise lithiation behavior is explained through our theoretical analysis, which appears well-aligned with the experimental evidence.

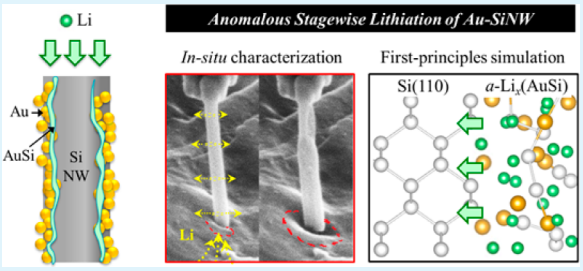

KEYWORDS: *gold-coated silicon nanowire, stagewise lithiation, in situ characterization, density functional theory calculation, lithium ion battery*

INTRODUCTION

Since its commercialization in 1991, lithium (Li)-ion batteries have become the most popular power source for portable electronics because they have high energy and power density, no memory degradation effects, and only limited self-discharge.[1,2] Still, this technology can be improved in many aspects in order to fulfill the emerging and most demanding applications like electric vehicles and large-scale renewable energy storage, which require much higher energy density, faster charge/discharge rates, and better long-term cyclability. Among many innovative solutions,[3−15] a possible approach to simultaneously increase the energy and power densities of a Li-ion battery is demonstrated via utilizing nanostructured (Si) anode, like Si nanowires (SiNWs). Si-based materials have recently emerged as a promising anode because its abundance, environmental benignity and most importantly the highest known Li storage capacity (3579 mAh g^{-1}), nearly ten times larger than that of graphite (372 mAh g^{-1}), which leads to the significant increase in energy density.[16,17] Moreover, the one-dimensional nanostructure provides not only the mechanical strength and flexibility to accommodate the large volume variation during cycling, but also the facile lithiation/delithiation path along surfaces; these merits together contribute to the impressive cycle stability at rapid charge/discharge rates.[18] Cho and Picraux have reported SiNW-based anodes exhibiting 1100 mAh g^{-1} discharge capacity after 1000 cycles at a 0.5C cycling rate, and higher than 900 mAh g^{-1} at 10C.[19] With further nanostructuring, hollow Si nanotubes by Cui and Wu could maintain a 1000 mAh g^{-1} discharge capacity even after 6000 cycles at a 12C rate.[20]

One common approach to grow SiNWs is via the vapor−liquid−solid (VLS) process with gold (Au) catalysts.[21,22] In the VLS growth, a significant amount of Au was found to spread on the NW sidewalls.[23,24] The presence of Au may influence the physical properties of SiNWs and also modify the NW morphology.[23,24] In addition, for Li-ion battery anodes, we thought that metallic Au would be an intriguing choice of coating material for SiNWs because of the following reasons: (i) Au is also reactive toward Li with a capacity of 451 mAh g^{-1} (based on lithiated intermetallic compound of $Li_{15}Au_4$),[25] (ii) Au is mechanically ductile and electrically conductive, hence being able to maintain both the structural stability and conductive path, and (iii) it has been shown that Au−Si alloys are likely to form at the Au/Si interface,[26−28] which may in turn introduce intricate interfacial effects that influence the lithiation behavior.

Recently, a few studies have touched on lithiation of Au-coated porous Si films[29] and SiNWs with residual gold seed particles,[30] where the effects of having the Au secondary phase were briefly mentioned. However, to the best of our knowledge,

Received: March 3, 2015
Accepted: July 21, 2015
Published: July 21, 2015

DOI: 10.1021/acsami.5b01930
ACS Appl. Mater. Interfaces 2015, 7, 16976−16983

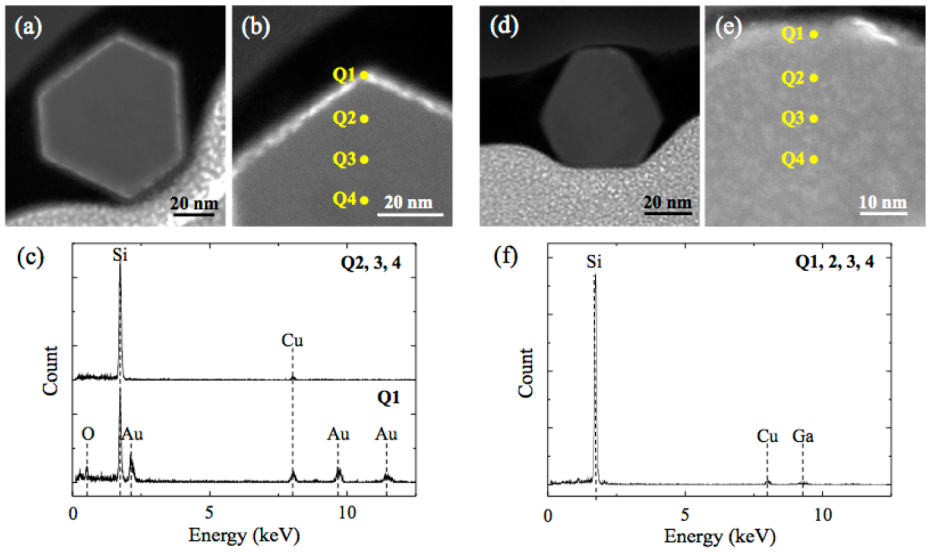

Figure 1. Surface characterization of Au-catalyzed Si NWs before and after HF etching. (a, b) HAADF-STEM images and (c) EDS analysis of the cross-section of an [111] Si NW before HF etching (i.e., Au-coated SiNW). The bright thin outer layer (Q1) as observed in (a, b) is attributed to Au dispersion, which is confirmed by the EDS spot analyses (Q1-Q4) presented in c. (d, e) and (f) are respectively the corresponding HAADF-STEM images and EDS analysis for a [111] SiNW after HF etching (i.e., without the presence of Au).

no atomistic-scale study either experimentally or computationally has been reported regarding the lithiation behavior of SiNWs that are covered by an appreciable amount of Au (hereon referred to as Au-SiNWs). Similarly, the idea of applying surface coatings on SiNWs with materials ranging from active (toward Li) C,[31] Ge,[32] Al,[33] to inactive Cu[34] and Ni[35] metals, and various oxides, TiO_2,[36] Al_2O_3,[37] and SiO_2[38] has been experimented before; the coated SiNWs have been found to often exhibit improved cycling and rate performance. But again, it is unclear how surface-modified SiNWs may undergo different structural evolution during lithiation, let alone underlying lithiation mechanisms and properties at the atomistic level.

In the paper, we present a combined experimental and theoretical investigation on lithiation in individual Au-SiNWs to better understand the impacts of having significant Au-spreading on the SiNW surface. An Au-SiNW is brought to direct contact with Li metal inside a scanning microscope, and its structural evolution during lithiation is characterized in situ. The lithiation process of an Au-SiNW appears to occur in three distinct stages, which is intriguingly different from that of an Au-free SiNW. The underlying mechanism for the "stagewise" lithiation behavior is examined using a first-principles computational approach to provide a rational explanation for our experimental observations. On the basis of density functional theory (DFT) calculations, we present how Li atoms are incorporated in Au-SiNW as a function of Li content, along with a detailed analysis of the lithiation energetics and dynamics, with special attention to the effects of the Au coating.

RESULTS AND DISCUSSION

Experimentally Observed Stagewise Lithiation of Au-SiNW. Figure 1a, b shows the high-angle annular dark field (HAADF)−scanning transmission electron microscope (STEM) micrographs of the cross-section (perpendicular to the nanowire axial) of an as-grown [111] SiNW bounded by six {110} sidewalls. As HAADF imaging is highly sensitive to atomic-number (Z) contrast, we are able to differentiate SiNW (the dark hexagon) from Au, which is visible as the bright outer layer of the hexagon. Consistently, results from the energy dispersive spectroscopy (EDS) analysis (Figure 1c) confirm the presence of Au at the outer layer [corresponding to Q1 in (Figure 1b), whereas only Si peaks are dominating the spectra toward the center of the NW (Q2, Q3, and Q4). Thus, it is clear that the surfaces of the as-grown SiNWs are covered by an appreciable amount of Au, which is typically observed in SiNWs grown by Au-seeded VLS process.[23,24] In the rest of this article, the SiNW with Au spreading at the surface will be referred to as "Au-SiNW". We confirmed that the Au spreading on the surface can be effectively removed by the surface treatment. For comparison, Figure 1d, e shows the HAADF-STEM images of the cross-section of the [111] SiNW after hydrofluoric acid (HF) etching. The bright sides present in Figure 1a, b no longer exist in d and e, and the results of EDS (Figure 1f) also confirm the absence of Au on the surface. The surface-treated SiNW will be referred to as "SiNW".

Next, the Au-SiNW was brought into direct contact with Li metal inside a scanning electron microscopy (SEM) in the absence of an applied electric field. Upon lithiation, the structural evolution is monitored in situ and shown in Figure 2. At t = 0.00 s, the Au-SiNW was straight with a uniform diameter around 96.2 nm. Once the Au-SiNW contacted bulk Li, the morphological changes are captured in the time-lapse series of SEM images up to t = 15.57 s, and the transformation of the lithiated Au-SiNW appears to occur in distinct stages (Stages I, II, and III). In Stage I, from t = 0−7.13 s, Li atoms near the vicinity of the contacting area underwent diffusion into the Au-SiNW accompanied by small radial volume expansion as the effective reaction front (marked by the yellow triangle) propagated from the nanowire tip toward the other end, along the "axial direction". In Stage II, the lithiation front had propagated through the entire length while the continuing lithiation process lead to slow and uniform volume expansion in the "radial direction" around t = 9.17−11.22 s. Finally, in Stage III, the entire Au-SiNW appeared to swell uniformly at once in the "radial direction" and reached the fully lithiated phase (corresponding to ∼417% volume expansion) within approx-

DOI: 10.1021/acsami.5b01930
ACS Appl. Mater. Interfaces 2015, 7, 16976−16983

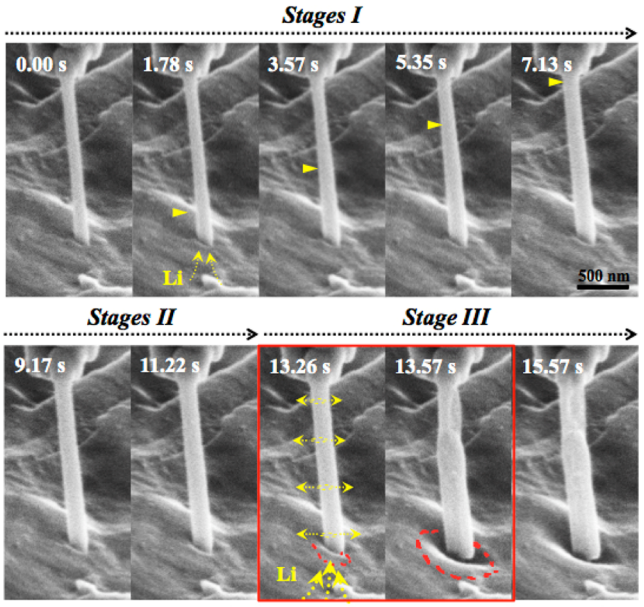

Figure 2. Temporal microstructure evolution of an [111] Au-SiNW in direct contact with Li metal, which clearly demonstrates a stagewise lithiation behavior; the elapsed time during lithiation is indicated in second (s). In Stage III, volume expansion tends to occur instantaneously as the effective reaction front (marked by the yellow triangle) propagated from the nanowire tip toward the other end. The dotted red line indicates the bulk Li surface in the vicinity of the contacting area drastically sunk down due to the rapid Li diffusion into the Au-SiNW.

imately one second (t = 13.26−13.57 s). As indicated by the dotted red line, the bulk Li surface in the vicinity of the contacting area drastically sunk down because Li atoms rapidly diffused into the Au-SiNW. These results highlight an intriguingly different lithiation behavior of Au-SiNW as compared to conventional SiNWs without residual Au coverage at the surfaces.[8,18,30] To better understand how the lithiation behavior is influenced by the presence of Au on the surfaces of SiNWs, we carried out DFT calculations to investigate the lithiation mechanism of Au-SiNWs at atomistic level.

Single Li Incorporation in Au-SiNW. According to our experimental observations as discussed in the previous section, the as-grown SiNW is covered with a thin layer of Au.[23,24] We could also expect that Au and Si are alloyed to form an AuSi interface layer, considering previous experimental and theoretical results; it has been found that the AuSi alloy exhibits a negative mixing enthalpy and Au deposition on a Si substrate leads to Au-silicide formation.[28] Provided an Au-SiNW consists of Si core, AuSi interface, and Au shell, to understand its lithiation behavior it would be necessary to assess the incorporation and diffusion of Li atoms in these three different phases.

We first calculated the formation (E_f) and migration (E_m) energies of a single Li atom in Au, AuSi, and Si (summarized in Table 1).

In face-centered-cubic (fcc)-Au, a Li atom could possibly be incorporated at an octahedral or tetrahedral site with E_f (Li_O) = 0.72 eV or E_f (Li_T) = 1.31 eV, respectively; here, E_f is calculated with respect to bcc-Li (E_{Li}) and *fcc*-Au host (E_{Au}), i.e., $E_f = E_{Li+Au} - E_{Li} - E_{Au}$, where E_{Li+Au} is the total energy of one Li interstitial in 64-atom *fcc*-Au. However, given that the vacancy formation energy in fcc-Au is relatively low ($E_f(V_{Au}) \approx 0.41$ eV from our DFT-PW91 calculations),[39] there may exist a considerable amount of vacancies. In this case, Li atoms can be incorporated into the substitutional (vacancy) sites with the predicted E_f (Li_{Au}) of −1.04 eV including the vacancy formation energy, (i.e., $E_f(Li_{Au}) = E_{Li_{Au}} - E_{Li} - E_{V_{Au}} + E_f(V_{Au})$, where $E_{Li_{Au}}$ and $E_{V_{Au}}$ are the total energies of the 64-atom fcc-Au with an Li atom at the substitutional site and with an Au vacancy, respectively). These calculations clearly evidence that Li insertion in fcc-Au is energetically the most favorable at a substitutional site, which is consistent with previous experiments.[40−42]

Table 1. Calculated Formation (E_f) and Migration (E_m) Energies of a Single Li Atom in Au, AuSi, and Si

host		species	E_f (eV)	E_m (eV)
crystalline	Au	Li_O	0.72	
		Li_T	1.31	
		Li_{Au}	− 1.04	
		Li_{Au}-V_{Au}	− 0.73	0.29
	Si	Li_T	0.31	0.62
amorphous	Au		−1.29 ± 0.31	1.11 ± 0.42
	AuSi	Li	−1.31 ± 0.42	0.66 ± 0.33
	Si		−0.01 ± 0.24	0.45 ± 0.21

For Li insertion in crystalline Si (*c*-Si), the tetrahedral interstitial site is identified to be energetically the most favorable with E_f (Li_T) = 0.31 eV, and the E_f value is found to decrease significantly to −0.01 ± 0.24 eV in its amorphous phase (*a*-Si) because of the more flexible lattice. Unlike the covalently bonded Si matrix, there is a significant reduction in E_f in the metallic *a*-Au (E_f = −1.29 ± 0.31 eV) and *a*-AuSi (E_f = −1.31 ± 0.42 eV) matrices, implying that Li can be easily accommodated in the *a*-Au and *a*-AuSi structures with no significant energy cost.

Next, we evaluated the variations in the Li migration barrier (E_m) as the host material changes. In *c*-Si, the predicted E_m for Li interstitial is 0.62 eV.[43] In fcc-Au, a substitutional Li may undergo migration by exchanging its position with a neighboring Au atom or vacancy (if exists). While the former requires overcoming a very high barrier, the latter is predicted to occur with a moderate (vacancy-mediated) barrier of E_m (Li_{Au}-V_{Au}) = 0.29 eV; here, the formation energy for the Li substitutional and Au vacancy pair can be estimated to be E_f (Li_{Au}-V_{Au}) = −0.73 eV = $E_{Li_{Au}}$-$V_{Au} - E_{Li} - [(N-2)/N]E_{Au}$, where $E_{Li_{Au}}$-V_{Au} is the total energy of one Li_{Au}-V_{Au} pair in 64-atom fcc-Au (N = 64). However, in the amorphous phases of Si (*a*-Si) and Au (*a*-Au), the predicted E_m values are 0.45 ± 0.21 eV and 1.11 ± 0.42 eV, respectively; interestingly, the E_m of 0.66 ± 0.33 eV for a Li atom in *a*-AuSi is in between those for the *a*-Si and *a*-Au cases.

Looking at the E_f and E_m values in the different phases considered (*c*-Au, *a*-Au, *a*-AuSi, *c*-Si, *a*-Si), it is important to note that despite the relatively larger E_m in Au and AuSi, the significantly smaller E_f contribute to the smaller relative activation energy ($E_a = E_f + E_m$) for lithiation overall. The relative E_a with respect to that of *c*-Si for different phases from the most to least favorable are ΔE_a = −1.58 eV (*a*-AuSi) > −1.11 eV (*a*-Au) ≈ −1.37 eV (*c*-Au) > −0.44 eV (*a*-Si) > 0 eV (*c*-Si); note that the lower ΔE_a corresponds to the lower energy cost for Li incorporation and diffusion. This analysis may suggest that, upon lithiation of an Au-coated SiNW, Li atoms would be preferentially incorporated along the *a*-AuSi interface

DOI: 10.1021/acsami.5b01930
ACS Appl. Mater. Interfaces 2015, 7, 16976−16983

(Stage I) assuming the *a*-AuSi interface is sufficiently thick. Then, as lithiation progresses, Li atoms could advance into the Au layer (Stage II), rather than the Si layer, as its lattice near the Au/AuSi interface is somewhat disordered already due to the interface formation and disturbance from the expanded (lithiated) AuSi. At the very last, the Si core region would be lithiated (Stage III). Contrarily, if the *a*-AuSi interface layer were rather thin, lithiation of an Au-SiNW would be observed as a two-stage process: the outer Au (together with thin AuSi) layer is lithiated first, followed by lithiation of the Si-core. In either case, our calculations demonstrate that the priority of Au-/AuSi- vs. Si-lithiation is an intricate interplay between their corresponding E_f and E_m, which may in turn explain the stagewise lithiation behavior observed in an Au-SiNW.

Energetics and Dynamics of Lithiated Au-SiNW. In the previous section, we discussed the behavior of single Li atom in Au, AuSi, and Si. Here, we will look at the energetics and dynamic properties of their lithiated *a*-Li$_x$M alloys (M = Au, AuSi, Si and x = 0−3.57). Note that only the amorphous phases are considered (instead of their crystalline counterparts) because the Si and Au matrices lithiated beyond the first charge/discharge cycle are most likely to remain in the amorphous phase because of the sizable kinetic barrier for recrystallization.[44,45] We first calculated the E_f of *a*-Li$_x$M alloys to evaluate their relative stabilities with respect to body centered cubic (bcc)-Li and *a*-M host. The E_f per host atom is given by $E_f = E_{Li_xM} - (xE_{Li} + E_M)$, where E_{Li_xM} and E_M are the total energies per M atom of the *a*-Li$_x$M and *a*-M systems and E_{Li} is the per-atom energy of bcc-Li.

Figure 3 shows the variations in E_f as a function of x; for each alloy composition, the reported average value was obtained

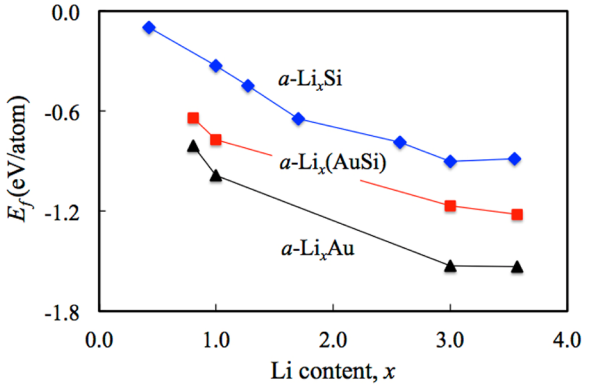

Figure 3. Formation energies (E_f) for *a*-Li$_x$Si, *a*-Li$_x$(AuSi), and *a*-Li$_x$Au alloys calculated on the basis of three different samples for each composition.

based on three independent 64-atom samples. For both *a*-Li$_x$Si and *a*-Li$_x$Au alloys, E_f continue to decrease with increasing Li content, and fall to plateaus between x = 3 and 4, corresponding to the fully lithiated composition. The E_f of *a*-Li$_x$Au is lower than that of *a*-Li$_x$Si, indicating Au lithiation is energetically more favorable than Si lithiation. We also checked the E_f for lithiated *a*-AuSi, which tends to follow the same trend with increasing x while the values are falling in between that of *a*-Li$_x$Si and *a*-Li$_x$Au. These results indicate that it is energetically more favorable to lithiate Au (and AuSi) than Si to a ratio of Li:M ≈ 4; note also that, at the onset of lithiation, Li atoms are more favorably incorporated into Au (and AuSi) than Si, as discussed in the previous section. Therefore, we can expect that lithiation of Au-SiNW would initiate from the outer Au (and AuSi) shell, and once saturated, further lithiation proceeds into the Si core. Furthermore, we think that the highly stable *a*-Li$_x$Au alloy formation can lead to considerable Li trapped in the Au shell during the delithiation process; thus the irreversible capacity loss if the amount of Au on SiNW was excessive, which is consistent with previous experimental observations.[30]

Next, we examined how the room-temperature diffusivity of Li (D_{Li}) varies in moderately lithiated *a*-Li$_x$*M* alloys (x = 1). For each case, three samples were averaged to calculate the mean-square displacements (MSD) of Li atoms at each temperature; MSD = $|R_i(t) - R_i(0)|^2$, where $R_i(t)$ is the position of atom i at time t. On the basis of the MSD profiles, D_{Li} values were obtained using the Einstein relation, $D = \langle MSD \rangle / 6t$; the angular bracket denotes ensemble average over the ab initio molecular dynamics (AIMD) interval. The MD duration of 8 ps (ps) appears to be sufficient to obtain well-converged results; disregarding the first 2 ps, linear fits over a time interval of the following 6 ps yield the D_{Li} values.[46] Using these calculated D_{Li} values at different temperatures, an Arrhenius plot of $\ln(D_{Li})$ versus $1000/T$ is constructed based on $D = D_0 \exp(-E_m/kT)$ as shown in Figure 4; the estimated prefactor D_0, migration barrier E_m, and room-temperature diffusivity D_{Li} values are summarized in the inset table.

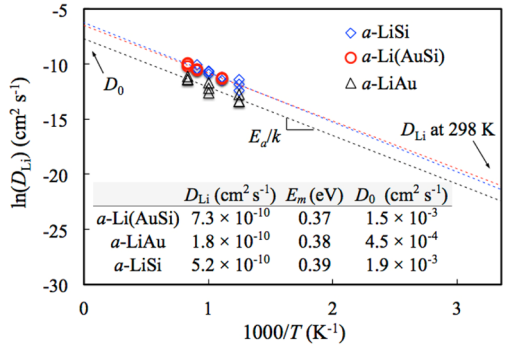

Figure 4. Arrhenius plot based on the predicted D_{Li} values *a*-LiSi, *a*-Li(AuSi), and *a*-LiAu alloys at various temperatures ranging from 800 to 1200 K. The estimated room-temperature D_{Li}, migration barrier E_m, and prefactor D_0 values are summarized in the inset.

Contrary to Li diffusion at the onset of lithiation (E_m ≈ 0.45 eV [*a*-Si], 0.66 eV [*a*-Au], and 1.11 eV [*a*-AuSi]), which is highly host-material-sensitive, the E_m tends to be significantly reduced and becomes similar in value when the host is moderately lithiated (E_m ≈ 0.39 eV [*a*-LiSi], 0.38 eV [*a*-LiAu], 0.37 eV [*a*-Li(AuSi)]). The D_0 values are around 1 × 10^{-3} cm^2 s^{-1} for all three cases, which is comparable with the prediction based on the harmonic transition state theory.[47,48] Manifested by the comparable E_m and D_0, the room-temperature D_{Li} in the three moderately lithiated *a*-Li$_x$*M* alloys (x = 1) are of the same order of magnitude; D_{Li} = 5.2, 7.3, and 1.80 × 10^{-10} cm^2 s^{-1} in *a*-LiSi, *a*-Li(AuSi), and *a*-LiAu, respectively. For comparison, we also checked D_{Li} at 800 K as the Li content is further increased to x = 3.57, and D_{Li} again turn out to be very similar in value; D_{Li} = 2.8 ± 0.5, 3.7 ± 0.3, and 4.5 ± 1.4 × 10^{-5} cm^2 s^{-1} in *a*-Li$_{3.57}$Si, *a*-Li$_{3.57}$(AuSi), and *a*-Li$_{3.57}$Au, respectively. These results exhibit a clear trend: at the early stage of lithiation (x ≈ 0), Li diffusion is significantly faster in Au and AuSi than in Si, and upon further lithiation (i.e., x increases to 1.0 and 3.57), D_{Li} continue to increase in all three *a*-Li$_x$*M* alloys and

DOI: 10.1021/acsami.5b01930
ACS Appl. Mater. Interfaces 2015, 7, 16976−16983

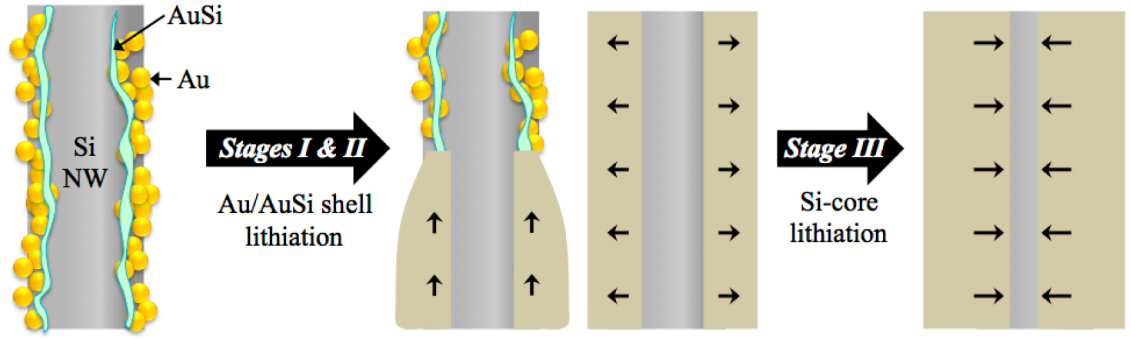

Figure 5. Proposed stagewise lithiation of an individual Au-SiNW. Stages I & II: axial lithiation of the Au shell with progressive and slow expansion while the AuSi interface layer may serve as a facile diffusion path. Stage III: radial lithiation of the Si-core with uniform and rapid expansion.

eventually approach comparable values in the highly lithiated phases. This is not surprising given that the host materials would be softened, undergo significant disintegration during lithiation, and ultimately reach final lithiated phases that are Li-rich alloys with similar properties regardless of the original material characteristics of M.[43,49,50]

Proposed Mechanism for Stagewise Lithiation in Au-Coated SiNW. On the basis of the aforedescribed simulation results, we propose a mechanism for the intriguing stagewise lithiation in an individual Au-coated SiNW, as illustrated in Figure 5.

- Stages I & II: Axial lithiation of the Au shell with progressive and slow expansion: As presented above, Li atoms are predicted to be incorporated preferentially in the Au shell, whereas the AuSi interface layer (provided it is sufficiently thick) may serve as a facile diffusion path at the early stage of lithiation. As the lithiation front proceeds in the axial direction through the entire Au shell, the lithiated region exhibits a gradual radial expansion until the full lithiation capacity of Au (≈ a-Li_4Au) is nearly reached.
- Stage III: Radial lithiation of the Si-core with uniform and rapid expansion: Once the Au shell is close to fully lithiated in Au-coated SiNW, Li atoms may start diffusing into the Si core, as a-Li_xAu alloys are far more stable than a-Li_xSi alloys; this is also well-demonstrated by our simulation results in Figure 6. The radial diffusion of Li atoms into the Si core leads to the spontaneous formation of a-Li_xSi alloys. Because the diffusion distance in the radial direction is significantly shorter than in the axial direction, the corresponding radial expansion appears to occur much more rapidly and simultaneously over the entire NW length.

To verify that the transition to Stage III can occur only after the Au/AuSi shell is highly (or close to fully) lithiated, we performed additional AIMD simulations to examine how Li atoms undergo diffusion across an a-Li_x(AuSi)/Si(110) interface. Here, we considered x = 0.8 and 3.57 representing the relatively earlier and later parts of Stage I, where the Au sell (together with the AuSi interface) is moderately and highly lithiated, respectively. The a-Li_x(AuSi)/Si(110) model systems were annealed at 1000 K, while the spreading of Li atoms in each system was analyzed as the simulation time progresses; the annealing temperature of 1000 K was chosen such that the thermal energy is sufficient to agitate atomic movements but far below the melting point of c-Si.

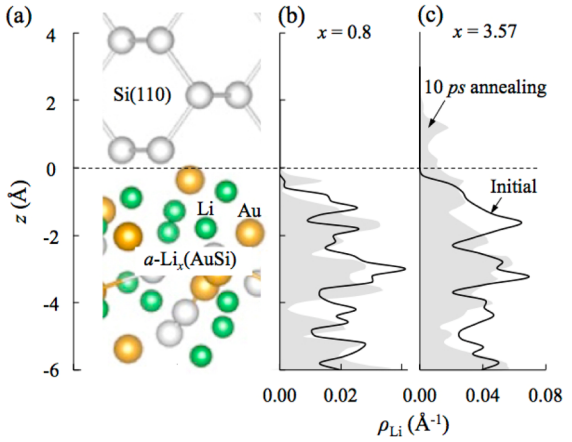

Figure 6. (a) Schematic of the supercell of a-Li_x(AuSi)/Si(110) interface, where x = 0.8 and 3.57. (b, c) are the number density (ρ_N) profiles of Li along the direction normal to the a-Li_x(AuSi)/Si(110) interface before and after 10 ps of annealing for x = 0.8 and 3.57, respectively.

Figure 6 compares the number density (ρ_N) profiles of Li along the direction normal to the a-Li_x(AuSi)/Si(110) interface before and after 10 *ps* annealing. At x = 0.8 (b) (i.e., the Au-shell is only moderately lithiated), there is no significant Li spreading into the Si core region even over the relatively long period of high temperature (= 1000 K) annealing. Contrarily, as the Li content increases to x = 3.57 (c) in the Au-shell (almost fully lithiated), a significant amount of Li atoms are found to diffuse into the Si core region. These results demonstrate that lithiation of the Si core may take place mainly after the Au-shell is highly lithiated, which is in line with our proposed stagewise lithiation behavior for Au-coated SiNW as also consistent with the afore-discussed experimental observations (Figure 2).

CONCLUSIONS

In this study, we employed a combined effort of in situ SEM experiments and DFT calculations to investigate the lithiation behavior of individual Au-SiNW, with particular attention to the effects of the Au coating. Upon direct contact with Li metal, the Au-SiNW appeared to be lithiated in three distinct stages, which is intriguingly different from that of a lithiated SiNW. First, we observed a clear lithiation front propagating from the tip to base of the Au-SiNW along the axial direction; followed by which was the slow and uniform expansion of the Au-SiNW in the radial direction, and finally, the entire Au-SiNW suddenly

DOI: 10.1021/acsami.5b01930
ACS Appl. Mater. Interfaces 2015, 7, 16976−16983

swelled uniformly in the radial direction to its fully lithiated volume (about 400%).

The underlying mechanism for the "stagewise" lithiation behavior was then examined based on DFT calculations. First, we found that at the onset of lithiation, the order of Li incorporation is dependent on the intricate interplay between the formation (E_f) and migration (E_m) energies of a single Li atom in Au, AuSi and Si, given the reasonable assumption that Au-SiNW is composed of an Au surface, a thin AuSi interface and the inner Si core. While E_f is the smallest in Au, followed by AuSi and the largest in Si, the corresponding E_m is in the opposite order. As the result, the overall activation energy ($E_a = E_f + E_m$) for lithiation, from the most to least favorable was predicted to be AuSi > Au > Si. Furthermore, we examined the energetics and dynamic properties of their lithiated amorphous a-Li$_x$$M$ alloys (M = Au, AuSi, Si and x = 0−3.57). In terms of the favorability of the alloy formation, a-Li$_x$Au was predicted to be the most stable, followed by a-Li$_x$(AuSi) and a-Li$_x$Si, and in either case, the Li/M ratio ($\approx$ 4) appears to reach the fully lithiated composition. We also predicted that as the host materials (M) undergo significant structural transformation and softening during lithiation, the Li diffusivities (D_{Li}) in a-Li$_x$$M$ become very similar in value ($\times$ 10^{-10} cm^2 s^{-1} at room temperature) regardless of their original material characteristics. That is at the early stage of lithiation ($x \approx 0$), Li diffusion is significantly faster in Au and AuSi than in Si, and upon further lithiation, D_{Li} continue to increase in all three a-Li$_x$M alloys and eventually approach comparable values in the highly lithiated phases.

Based on these results, the mechanism of the stagewise lithiation behavior could be explained as such. At the onset of lithiation (Stage I), Li atoms are incorporated preferentially in the Au shell while the AuSi interface may serve as a facile diffusion path, demonstrating clear propagation of the lithiation front along the axial direction. In Stage II, the Au shell (and AuSi interface) is lithiated at a steady rate accompanied by a gradual and uniform radial expansion until the full lithiation capacity of Au ($\approx$ a-Li$_4$Au) is nearly reached. At some point, the Au shell reaches its full lithiation capacity, and Li atoms begin to promptly diffuse into the Si core, leading to the sudden radial expansion of Au-SiNW in the last stage, Stage III. AIMD simulations were also performed to examine how Li atoms undergo diffusion across an lithiated a-Li$_x$(AuSi)/Si interface to verify the transition from Stages II to III after the Au (AuSi) shell is highly (or close to fully) lithiated.

The combined experimental and theoretical study clearly demonstrates and explains the intriguing stagewise lithiation behavior of Au-SiNW, where the effects of Au coating and Au/Si interface are prominent. The improved fundamental understandings may also contribute to the design of Si-based anodes with tailored lithiation behavior through calculated surface and interface engineering.

METHODS

In Situ Direct Contact Lithiation. The direct chemical lithiation test in the absence of an external electrical field and electrolyte was performed inside a focused ion beam (FIB) system (Quanta 3D, FEI).

A SiNW was fixed to the tungsten tip of the nanomanipulator (MM3A, Kleindiek) via Pt deposition. The SiNW was fractured inside the FIB chamber and brought into direct contact with Li metal, which was sliced by a microblade inside the FIB chamber to ensure the Si and Li contacting surfaces were both freshly exposed and free of oxidation. A schematic of the setup is illustrated in Figure 7a.

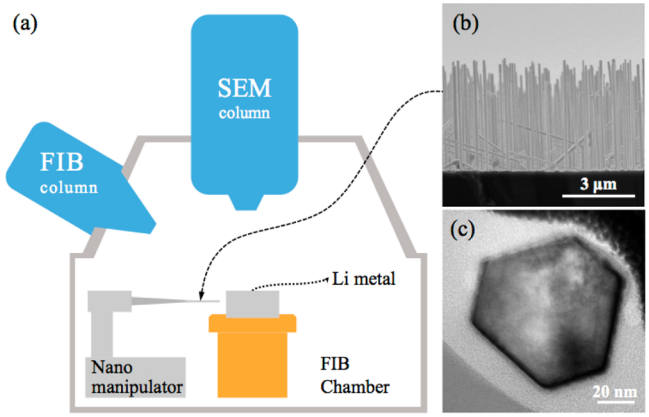

Figure 7. (a) Schematic of the experimental setup (with integrated dual-beam FIB/SEM) for the in situ characterization of Au-SiNW lithiation. (b) SEM image of [111] Au-SiNWs and (c) corresponding cross-section TEM image confirming the ⟨111⟩ axial orientation with six {110} sidewalls.

Fabrication of Single-Crystalline Si Nanowires with Au Coverage on the Surface. Au−Si droplets were synthesized on Si (111) substrates by depositing a 2 nm thick Au film (as catalyst) via thermal evaporation around 5 × 10^{-7} Torr, followed by a 5 min annealing step around 1 × 10^{-8} Torr. After this step, the vapor−liquid−solid (VLS) growth of Si NWs was carried out in an UHV-CVD system as the sample was exposed to a SiH_4:H_2 gaseous mixture under a pressure of 2 Torr at the Au−Si eutectic temperature (400−450 °C). It is worth noting that followed by the VLS growth, the Au catalysts can be removed via a surface treatment process using dilute hydrofluoric acid (HF) solutions, but this step was deliberately omitted for the purpose of this study. The morphology of the SiNWs was observed by scanning electron microscopy (SEM, Quanta 3D, FEI); as shown in Figure 7b, the as-grown SiNWs are approximately 70−110 nm in diameter and 3−4 μm in length. The structure of individual SiNWs was characterized using a transmission electron microscope (TEM, Titan 80−300, FEI). Figure 7c shows the cross-section TEM image, confirming the ⟨111⟩ axial orientation of the SiNW with six {110} sidewalls. Furthermore, individual SiNWs was also characterized using a scanning transmission electron microscope (STEM, Titan 80−300, FEI) and high-angle annular dark-field (HAADF) imaging (also called Z-contrast) along with energy-dispersive spectroscopy (EDS) analysis to examine the presence/distribution of the Au catalysts.

Computational Methods. Quantum mechanical calculations reported herein were performed on the basis of density functional theory (DFT) within the generalized gradient approximation with the Perdew−Wang-91 exchange-correlation functional (GGA-PW91),[51] as implemented in the Vienna Ab-initio Simulation Package (VASP).[52−54] The projected augmented wave (PAW) method with a plane-wave basis set was used to describe the interaction between core and valence electrons. An energy cutoff of 300 eV (350 eV) was used for geometric optimization of the crystalline (amorphous) model structures; all atoms were fully relaxed using the conjugate gradient method until residual forces are smaller than 5 × 10^{-2} eV Å^{-1}. The model structures of amorphous Li$_x$Si, Li$_x$(AuSi) and Li$_x$Au alloys, each containing total 64 atoms, were created using ab initio molecular dynamics (AIMD) simulations following the same procedures as described in ref 55. The initial structure for the a-Li$_x$(AuSi)/Si(110) interfaces (x = 0.8 and 3.57) were prepared by stacking a 64-atom a-Li$_x$(AuSi) bulk model on top of a 48-atom c-Si supercell in the [110] direction. The a-Li$_x$(AuSi)/Si(110) systems were fully relaxed and then annealed at 500 K for 1 ps to allow sufficient atomic rearrangement, followed by geometry optimization. The Monkorst-Pack scheme[56] was used for Brillouin zone sampling with sufficient k-points for the corresponding model structure as summarized in Table 2.

DOI: 10.1021/acsami.5b01930
ACS Appl. Mater. Interfaces 2015, 7, 16976−16983

Table 2. Monkhorst−Pack *k*-Point Meshes Used for the Brillouin Zone Sampling of the Model Structures Considered in This Work

model structure	*k*-mesh
c-Si (*a* = 5.457 Å)	4 × 4 × 4
c-Au (*a* = 4.173 Å)	6 × 3 × 6
a-M (M = Si, AuSi, Au)	2 × 2 × 2
a-Li_xM (M = Si, AuSi, Au)	2 × 2 × 2
a-Li_x(AuSi)/Si(110)	Γ-centered 1 × 1 × 1

AUTHOR INFORMATION

Corresponding Authors

*E-mail: insukchoi@kist.re.kr.

*E-mail: gshwang@che.utexas.edu.

Author Contributions

†C.-Y.C. and J.-H.S. contributed equally to this work.

Notes

The authors declare no competing financial interest.

ACKNOWLEDGMENTS

This work was supported in part by the Robert A. Welch foundation (Grant F-1535) (GSH) and KIST R&D program of 2Z04520, MSIP/NST R&D Convergence Program (Grant Yunghap-13-1-KIST) (ISC). We also thank the Texas Advanced Computing Center for use of their computing resources.

REFERENCES

(1) Nishi, Y. Lithium Ion Secondary Batteries. Past 10 Years and the Future. *J. Power Sources* **2001**, *100*, 101−106.

(2) Tarascon, J.-M.; Armand, M. Issues and Challenges Facing Rechargeable Lithium Batteries. *Nature* **2001**, *414*, 359−367.

(3) Netz, A.; Huggins, R. A.; Weppner, W. The Formation and Properties of Amorphous Silicon as Negative Electrode Reactant in Lithium Systems. *J. Power Sources* **2003**, *119-121*, 95−100.

(4) Bourderau, S.; Brousse, T.; Schleich, D. M. Amorphous Silicon as a Possible Anode Material for Li-Ion Batteries. *J. Power Sources* **1999**, *81−82*, 233−236.

(5) Hatchard, T. D.; Dahn, J. R. In Situ XRD and Electrochemical Study of the Reaction of Lithium with Amorphous Silicon. *J. Electrochem. Soc.* **2004**, *151*, A838−A842.

(6) Gao, B.; Sinha, S.; Fleming, L.; Zhou, O. Alloy Formation in Nanostructured Silicon. *Adv. Mater.* **2001**, *31*, 816−819.

(7) Graetz, J.; Ahn, C. C.; Yazami, R.; Fultz, B. Highly Reversible Lithium Storage in Nanostructured Silicon. Electrochem. *Electrochem. Solid-State Lett.* **2003**, *6*, A194−A197.

(8) Chan, C. K.; Peng, H.; Liu, G.; McIlwrath, K.; Zhang, X. F.; Huggins, R. A.; Cui, Y. High Performance Lithium Battery Anode Using Silicon Nanowires. *Nat. Nanotechnol.* **2008**, *3*, 31−35.

(9) Beaulieu, L. Y.; Hewitt, K. C.; Turner, R. L.; Bonakdarpour, A.; Abdo, A. A.; Christensen, L.; Eberman, K. W.; Krause, L. J.; Dahn, J. R. The Electrochemical Reaction of Li with Amorphous Si-Sn Alloys. *J. Electrochem. Soc.* **2003**, *150*, A149−A156.

(10) Mao, O.; Turner, R. L.; Courtney, I. A.; Fredericksen, B. D.; Buckett, M. I.; Krause, L. J.; Dahn, J. R. Active/inactive Nanocomposites as Anodes for Li-Ion Batteries. *Electrochem. Solid-State Lett.* **1999**, *2*, 3−5.

(11) Fleischauer, M. D.; Topple, J. M.; Dahn, J. R. Combinatorial Investigations of Si-M (M = Cr + Ni, Fe, Mn) Thin Film Negative Electrode Materials. *Electrochem. Solid-State Lett.* **2005**, *8*, A137−A140.

(12) Ghassemi, H.; Au, M.; Chen, N.; Heiden, P. A.; Yassar, R. S. In-situ Lithiation/Delithiation Observation of Individual Amorphous Si Nanorods. *ACS Nano* **2011**, *5*, 7805−7811.

(13) Yang, J.; Winter, M.; Besenhard, J. O. Small Particle Size Multiphase Li-alloy Anodes for Lithium-Ion-Batteries. *Solid State Ionics* **1996**, *90*, 281−287.

(14) Huggins, R. A.; Nix, W. D. Decrepitation Model for Capacity Loss during Cycling of Alloys in Rechargeable Electrochemical Systems. *Ionics* **2000**, *6*, 57−63.

(15) Li, J.; Dozier, A. K.; Li, Y.; Yang, F.; Cheng, Y.-T. Crack Pattern Formation in Thin Film Lithium-ion Battery Electrodes. *J. Electrochem. Soc.* **2011**, *158*, A689−A694.

(16) Sharma, R. A.; Seefurth, R. N. Thermodynamic Properties of the Lithium-silicon System. *J. Electrochem. Soc.* **1976**, *123*, 1763−1768.

(17) Boukamp, B. A.; Lesh, G. C.; Hggins, R. A. All-solid Lithium Electrodes with Mixed-Conductor Matrix. *J. Electrochem. Soc.* **1981**, *128*, 725−729.

(18) Zamfir, M. R.; Nguyen, H. T.; Moyen, E.; Lee, Y. H.; Pribat, D. Silicon Nanowires for Li-Based Battery Anodes; A Review. *J. Mater. Chem. A* **2013**, *1*, 9566−9586.

(19) Cho, J.-H.; Picraux, S. T. Enhanced Lithium Ion Battery Cycling of Silicon Nanowire Anodes by Template Growth to Eliminate Silicon Underlayer Islands. *Nano Lett.* **2013**, *13*, 5740−5747.

(20) Wu, H.; Chan, G.; Choi, J. W.; Ryu, I.; Yao, Y.; McDowell, M. T.; Lee, S. W.; Jackson, A.; Yang, Y.; Hu, L. B.; Cui, Y. Stable Cycling of Double-Walled Silicon Nanotube Battery Anodes Through Solid-Electrolyte Interphase Control. *Nat. Nanotechnol.* **2012**, *7*, 310−315.

(21) Wagner, R. S.; Ellis, W. C. The Vapor-Liquid-Solid Mechanism of Crystal Growth and Its Application to Silicon. *Trans. Metall. Soc. AIME* **1965**, *233*, 1053−1064.

(22) Putnam, M. C.; Filler, M. A.; Kayes, B. M.; Kelzenberg, M. D.; Guan, Y.; Lewis, N. S.; Eiler, J. M.; Atwater, H. A. Secondary Ion Bass Spectrometry of Vapor-Liquid-Solid Grown, Au-catalyzed, Si Wires. *Nano Lett.* **2008**, *8*, 3109−3113.

(23) Vincent, L.; Boukhicha, R.; Gardès, C.; Renard, C.; Yam, V.; Fossard, F.; Patriarche, G.; Bouchier, D. Faceting Mechanisms of Si Nanowires and Gold Spreading. *J. Mater. Sci.* **2012**, *47*, 1609−1613.

(24) Dailey, E.; Madras, P.; Drucker, J. Au on Vapor-Liquid-Solid Grown Si Nanowires: Spreading of Liquid AuSi from the Catalytic Seed. *J. Appl. Phys.* **2010**, *108*, 064320−064328.

(25) Yuan, L.; Liu, H. K.; Maaroof, A.; Konstantinov, K.; Liu, J.; Cortie, M. Mesoporous Gold as Anode Materials for Lithium-Ion Cells. *Aust. J. Chem.* **2007**, *10*, 95−99.

(26) Bokhonov, B.; Korchagin, M. In Situ Investigation of Stage of the Formation of Eutectic Alloys in Si-Au and Si-Al Systems. *J. Alloys Compd.* **2000**, *312*, 238−250.

(27) Wang, H.; Zepeda-Ruiz, L. A.; Gilmer, G. H.; Upmanyu, M. Atomistics of Vapour-Liquid-Solid Nanowire Growth. *Nat. Commun.* **2013**, *4*, 1956.

(28) Lee, S.-H.; Hwang, G. S. Structure, Energetics, and Bonding of Amorphous Au-Si Alloys. *J. Chem. Phys.* **2007**, *127*, 224710−1−5.

(29) Thakur, M.; Isaacson, M.; Sinsabaugh, S. L.; Wong, M. S.; Biswal, S. L. Gold-coated Porous Silicon Films as Anodes for Lithium Ion Batteries. *J. Power Sources* **2012**, *205*, 426−432.

(30) Chockla, A. M.; Bogart, T. D.; Hessel, C. M.; Klavetter, K. C.; Mullins, C. B.; Korgel, B. A. Influence of Gold, Binder and Electrolyte on Silicon Nanowire Performance in Li-ion Batteries. *J. Phys. Chem. C* **2012**, *116*, 18079−18086.

(31) Huang, R.; Fan, X.; Shen, W.; Zhu, J. Carbon-Coated Silicon Nanowire Array Films for High-Performance Lithium-ion Battery Anodes. *Appl. Phys. Lett.* **2009**, *95*, 133119.

(32) Song, T.; Cheng, H.; Choi, H.; Lee, J. H.; Han, H.; Lee, D. H.; Yoo, D. S.; Kwon, M. S.; Choi, J. M.; Doo, S. G.; Chang, H.; Xiao, J.; Huwang, Y.; Park, W. I.; Chung, Y. C.; Kim, H.; Rogers, J. A.; Paik, U. Si/Ge Double-Layered Nanotube Array as a Lithium Ion Battery Anode. *ACS Nano* **2012**, *6*, 303−309.

(33) Memarzadeh, E. L.; Kalisvaart, W. P.; Kohandehghan, A.; Zahiri, B.; Holt, C. M. B.; Mitlin, D. Silicon Nanowire Core Aluminum Shell Coaxial Nanocomposites for Lithium Ion Battery Anodes Grown with and without a TiN Interlayer. *J. Mater. Chem.* **2012**, *22*, 6655−6668.

DOI: 10.1021/acsami.5b01930
ACS Appl. Mater. Interfaces 2015, 7, 16976−16983

(34) Chen, H.; Xiao, Y.; Wang, L.; Yang, Y. Silicon Nanowires Coated with Copper Layer as Anode Materials for Lithium-Ion Batteries. *J. Power Sources* **2011**, *196*, 6657−6662.
(35) Sandu, G.; Brassart, L.; Gohy, J.-F.; Pardoen, T.; Melinte, S.; Vlad, A. Surface Coating Mediated Swelling and Fracture of Silicon Nanowires during Lithiation. *ACS Nano* **2014**, *8*, 9427−9436.
(36) Lotfabad, E. M.; Kalisvaart, P.; Cui, K.; Kohandehghan, A.; Kupsta, M.; Olsen, B.; Mitlin, D. ALD TiO_2 Coated Silicon Nanowires for Lithium Ion Battery Anodes with Enhanced Cycling Stability and Coulombic Efficiency. *Phys. Chem. Chem. Phys.* **2013**, *15*, 13646−13657.
(37) Nguyen, H. T.; Zamfir, M. R.; Duong, L. D.; Lee, Y. H.; Bondavalli, P.; Pribat, D. Alumina-Coated Silicon-Based Nanowire Arrays for High Quality Li-ion Battery Anodes. *J. Mater. Chem.* **2012**, *22*, 24618−24626.
(38) Sim, S.; Oh, P.; Park, S.; Cho, J. Critical Thickness of SiO_2 Coating Layer on Core@Shell Bulk@Nanowire Si Anode Materials for Li-Ion Batteries. *Adv. Mater.* **2013**, *25*, 4498−4503.
(39) $E_f(V_{Au}) = E_{V_{Au}} - ((N-1)/N)\ E_{Au}$, where $E_{V_{Au}}$ and E_{Au} are the total energies of the 64-atom *fcc*-Au with and without an Au vacancy, respectively; $N = 64$ was employed in this calculation.
(40) Pelton, A. D. The Au-Li (Gold-Lithium) System. *Bull. Alloy Phase Diagrams* **1986**, *7*, 228−231.
(41) Renner, F. U.; Kageyama, H.; Siroma, Z.; Shikano, M.; Schöder, S.; Gründer, Y.; Sakata, O. Gold Model Anodes for Li-ion Batteries: Single Crystalline Systems Studied by in Situ X-ray Diffraction. *Electrochim. Acta* **2008**, *53*, 6064−6069.
(42) Taillades, G.; Benjelloun, N.; Sarradin, J.; Ribes, M. Metal-Based Very Thin Film Anodes for Lithium Ion Microbatteries. *Solid State Ionics* **2002**, *152*−*153*, 119−124.
(43) Kim, H.; Kweon, K. E.; Chou, C.-Y.; Ekerdt, J. G.; Hwang, G. S. On the Nature and Behavior of Li Atoms in Si: A First Principles Study. *J. Phys. Chem. C* **2010**, *114*, 17942−17946.
(44) Obrovac, M. N.; Karuse, L. J. Reversible Cycling of Crystalline Silicon Powder. *J. Electrochem. Soc.* **2007**, *154*, A103−A108.
(45) Bach, P.; Seemayer, A.; Rütt, U.; Gutowski, O.; Renner, F. In Situ Observation of Lithium Alloying with Gold - Structural Details of Lithium Insertion/Extraction in/from Au Thin Film Electrodes for Lithium Ion Batteries. *2012 Annual Report of the Max-Planck-Institut Für Eisenforschung*. Retrieved from photon-science.desy.de/annual_report/files/2012/20122009.pdf.
(46) Chou, C.-Y.; Hwang, G. S. Surface Effects on the Structure and Lithium Behavior in Lithiated Silicon: A First Principles Study. *Surf. Sci.* **2013**, *612*, 16−23.
(47) $D_0 = \nu_0 a^2 \exp(-\Delta S/k)$, assuming ΔS (the entropy difference between the diffusing atom at the saddle point and the initial equilibrium state) is close to zero, ν_0 (the attempt frequency) $\approx 1 \times 10^{13}$ s^{-1} and a (the distance between adjacent hopping sites) $\approx 1 \times 10^{-8}$ cm, D_0 would be on the order of 1×10^{-3} cm^2/s.[54]
(48) Wang, X. R.; Xiao, X.; Zhang, Z. Apparent Anomalous Prefactor Enhancement for Surface Diffusion due to Surface Defects. *Surf. Sci.* **2002**, *512*, L361−L366.
(49) Chou, C.-Y.; Hwang, G. S. On the Origin of the Significant Difference in Lithiation Behavior between Silicon and Germanium. *J. Power Sources* **2014**, *263*, 252−258.
(50) Chou, C.-Y.; Kim, H.; Hwang, G. S. A Comparative First-Principles Study of the Structure, Energetics, and Properties of Li-M (M = Si, Ge, Sn) Alloys. *J. Phys. Chem. C* **2011**, *115*, 20018−20026.
(51) Blöchl, P. E. Projector Augmented-Wave Method. *Phys. Rev. B: Condens. Matter Mater. Phys.* **1994**, *50*, 17953−17979.
(52) Kresse, G.; Hafner, J. Ab Initio Molecular Dynamics for Liquid Metals. *Phys. Rev. B: Condens. Matter Mater. Phys.* **1993**, *47*, 558−561.
(53) Kresse, G.; Furthmuller, J. Efficiency of Ab-Initio Total Energy Calculations for Metals and Semiconductors Using a Plane-Wave Basis Set. *Comput. Mater. Sci.* **1996**, *6*, 15−50.
(54) Kresse, G.; Furthmuller, J. Efficient Iterative Schemes for Ab Initio Total-Energy Calculations Using a Plane-Wave basis set. *Phys. Rev. B: Condens. Matter Mater. Phys.* **1996**, *54*, 11169−11186.
(55) Kim, H.; Chou, C.-Y.; Ekerdt, J. G.; Hwang, G. S. Structure and Properties of Li-Si Alloys: A First-Principles Study. *J. Phys. Chem. C* **2011**, *115*, 2514−2521.
(56) Monkhorst, H. J.; Pack, J. D. Special Points for Brillouin-Zone Integrations. *Phys. Rev. B* **1976**, *13*, 5188−5192.

DOI: 10.1021/acsami.5b01930
ACS Appl. Mater. Interfaces 2015, 7, 16976−16983